

This discussion paper is/has been under review for the journal The Cryosphere (TC).
Please refer to the corresponding final paper in TC if available.

A wavelet melt detection algorithm applied to enhanced resolution scatterometer data over Antarctica (2000–2009)

N. Steiner and M. Tedesco

The City College of New York at the City University of New York, New York, NY, USA

Received: 4 May 2013 – Accepted: 12 May 2013 – Published: 14 June 2013

Correspondence to: N. Steiner (nsteiner@ccny.cuny.edu)

Published by Copernicus Publications on behalf of the European Geosciences Union.

Discussion Paper | Discussion Paper

Wavelet Snowmelt Algorithm over Antarctica

N. Steiner and
M. Tedesco

Title Page	
Abstract	Introduction
Conclusions	References
Tables	Figures
◀	▶
◀	▶
Back	Close
Full Screen / Esc	

[Printer-friendly Version](#)
[Interactive Discussion](#)



Abstract

Melting is mapped over Antarctica at a high spatial resolution using a novel melt-detection algorithm based on wavelets and multi-scale analysis. The method is applied to Ku band (13.4 GHz) normalized backscattering measured by SeaWinds on QuikSCAT and spatially enhanced on a 5 km grid over the operational life of the sensor (1999–2009). Wavelet-based estimates of melt spatial extent and duration are compared with those obtained by means of threshold-based detection methods, where melting is detected when the measured backscattering is 3 dB below the preceding winter mean value. Results from both methods are assessed by means of Automatic Weather Station (AWS) air surface temperature records. The yearly melting index, the product of melted area and melting duration, found using a fixed threshold and wavelet-based melt algorithm are found to have a relative difference within 7 % for all years. The majority of the difference between melting records determined from QuikSCAT are related to short-duration backscatter changes identified as melting using the threshold methodology but not the wavelet-based method. Compared with AWS records both methods show a relative accuracy to within 10 % based on estimated melt conditions using air temperatures. Melting maps obtained with the wavelet-based approach are also compared with those obtained from spaceborne brightness temperatures recorded by the Special Sensor Microwave/Image (SSMI). With respect to passive microwave records, we find a higher degree of agreement (9 % relative difference) for the melting index using the wavelet-based approach than threshold-based methods (11 % relative difference). Additionally, linkages between melting variability and the Southern Annular Mode (SAM), an important large-scale climate driver for Antarctica, are suggested by the results using wavelet based methods that are not found using threshold-based methods.

TCD

7, 2635–2678, 2013

Wavelet Snowmelt Algorithm over Antarctica

N. Steiner and
M. Tedesco

[Title Page](#)

[Abstract](#)

[Introduction](#)

[Conclusions](#)

[References](#)

[Tables](#)

[Figures](#)

◀

▶

[Back](#)

[Close](#)

[Full Screen / Esc](#)

[Printer-friendly Version](#)

[Interactive Discussion](#)



1 Introduction

The future response of the Antarctica Ice Sheet (AIS) to a changing climate is one of the largest uncertainties in the estimates and predictions of global sea-level rise over the coming decades (Hughes, 1981; Joughin and Alley, 2011; Overpeck et al., 2006; Shepherd and Wingham, 2007; Bromwich and Nicolas, 2010; Dowdeswell, 2006; Lemke et al., 2007). As temperature increases at high latitudes (e.g. Comiso, 2010; Hansen et al., 2010) the rate of surface melting is expected to increase (Ohmura, 2001). Analysis of long-term trends in weather station air-temperatures indicates a strongly positive trend in the duration of melting conditions over the Antarctic Peninsula (Vaughn, 2006; Barrand et al., 2013). Efforts to quantify mass balance indicate a positive trend in mass loss for much of the Western Antarctic Ice Sheet (WAIS) and the Antarctic Peninsula (AP) with a negative trend for much of the East Antarctic Ice Sheet (EAIS) (e.g. Chen et al., 2009; Rignot and Thomas, 2002; Shepherd and Wingham, 2007; Rignot et al., 2011). Recent results using a combined climate modelling and satellite observational approach suggest that in the period 1992 through 2011, the EAIS is gaining mass at a rate of $14 \pm 43 \text{ Gt yr}^{-1}$ while the Western Antarctic Ice Sheet and the Antarctic Peninsula exhibit a mass loss of, respectively, -65 ± 26 , and $-20 \pm 14 \text{ Gt yr}^{-1}$ (Shepherd et al., 2012).

In the recent past, the Antarctic Peninsula has experienced episodes of dramatic ice-shelf break-up, for example the 2002 Larsen B Ice Shelf and the 2008 Wilkins Ice Shelf collapses. Both were the consequence of a suite of physical surface processes as well as ocean-ice shelves interaction mechanisms, but with surface melting likely playing a key role. Indeed, the formation of meltwater ponds on the surface of the ice shelves caused by the accumulation of runoff might have contributed to the process of disintegration through hydro-fracturing (e.g., MacAyeal et al., 2003; Scambos et al., 2009). Instability caused by ice-shelf loss has been shown to increase observed ice flow velocity in related glacial tributaries (Rignot et al., 2004; Scambos et al., 2004;

[Title Page](#)[Abstract](#)[Introduction](#)[Conclusions](#)[References](#)[Tables](#)[Figures](#)[◀](#)[▶](#)[Back](#)[Close](#)[Full Screen / Esc](#)[Printer-friendly Version](#)[Interactive Discussion](#)

Rott et al., 2011). Melting also drives firn densification and compaction (Holland et al., 2011).

Direct measurements of melting are not available from in-situ data. Additionally, quantities necessary to fully solve the surface energy balance are often unavailable.

- 5 Therefore, surface melting is generally estimated from near-surface air temperature measurements performed by automatic weather stations (AWS), when and where available. Such measurements are sparse over Antarctica and mostly performed around coastal areas and at low elevations. Moreover, data measured from AWS represent only local conditions and are difficult to extrapolate or estimate melting at large spatial
10 scales without adding biases or increasing uncertainty.

Active microwave (AMW) and passive microwave (PMW) spaceborne instruments are used to monitor melting over snow covered areas due to the insensitivity to atmospheric and illumination conditions and high sensitivity to liquid water (e.g. Abdalati and Steffen, 2001; Ashcraft and Long, 2006; Liu et al., 2005; Mote et al., 1993; Nghiem
15 et al., 2007; Nghiem et al., 2001; Steffen et al., 2004; Tedesco et al., 2007; Torinesi et al., 2003; Wang et al., 2008). For vegetation-free snow covered areas, the volume scatter component will be dominant for radar backscatter measurements at Ku-band frequencies (Ulaby et al., 1986). Backscatter loss due to the presence of liquid water in snow during melting is responsible for a rapid and considerable decrease in the Ku-
20 band normalized microwave backscatter, σ^0 with respect to dry snow conditions. This is because of the increased imaginary component in the bulk complex dielectric constant of wet snow relative to dry snow (e.g. Ngheim and Tsai, 2001; Stiles and Ulaby, 1980). This same emissivity change will create near-blackbody emission characteristics for wet-snowpacks leading to a marked increase in brightness temperatures (Ulaby et al.,
25 1986; Stiles and Ulaby, 1980).

Various melt-detection algorithms have been developed and applied to active microwave (AMW) time-series to estimate seasonal melt. Often, a threshold value of absolute magnitude signal change either constant or regionally variable is used to detect melt-related changes (e.g. Ashcraft and Long, 2006; Trusel et al., 2012;

Wavelet Snowmelt Algorithm over Antarctica

N. Steiner and
M. Tedesco

Title Page

Abstract

Introduction

Conclusions

References

Tables

Figures

◀

▶

◀

▶

Back

Close

Full Screen / Esc

Printer-friendly Version

Interactive Discussion



Wavelet Snowmelt Algorithm over Antarctica

N. Steiner and
M. Tedesco

Wang et~al., 2008; Zwally and Fiegles, 1994). Generally, this threshold value is chosen as an approximation of the expected microwave response during snowmelt with respect to a baseline referring to wintertime dry snow conditions (e.g. Ashcraft and Long, 2006). We refer to all methods that consider a constant value threshold in the following as *fixed threshold* approaches (denoted FT thereafter). Alternately, approaches employing physically based temporal or spatially variable threshold values will be referred to as *dynamic threshold approaches* (Mote and Anderson, 1995; Tedesco, 2009). Algorithms that rely on the intrinsic properties of a measurement within time series have also been applied to snowmelt detection (Joshi et al., 2001; Liu et al., 2005; L. Wang and Yu, 2011). These approaches are dynamic in that they are based on the magnitude of relative change within each individual time-series. A *dynamic* approach assumes that large changes in the microwave region are associated with melting events so that “edges” are created in the backscattering time series. These edges can be identified and used to estimate the timing of melting events. Edge-detection algorithms of this type have been developed using derivative-of-Gaussian (DoG) (e.g. Yoshi et al., 2001) or multi-scale wavelet edge detection (Liu et al., 2006).

Building on previous *dynamic* melt-detection approaches (Yoshi et al., 2001; Liu et al., 2006), we introduce a wavelet-based melt detection algorithm based on multi-scale analysis of wavelet transforms to identify melting events using singularity detection (Mallet and Hwang, 1992). Such method identifies points of substantial transition in backscatter time-series using no a-priori information. In addition to this, a measure of the signal regularity at the point of transition can classify the transition “type”, which allows the separation of persistent melting events (melting lasting continuously for a certain number of days) from transient or sporadic melting events. Beside the wavelet-based approach, we also consider an FT algorithm-derived melting record from the same data-set. This FT record is to evaluate the wavelet-based method where alternative validation data, such as in-situ weather-station measurements, are not available. The FT method is performed as in Ashcraft et al.(2006) and Barrand et al. (2013).

[Title Page](#)

[Abstract](#) [Introduction](#)

[Conclusions](#) [References](#)

[Tables](#) [Figures](#)



[Back](#) [Close](#)

[Full Screen / Esc](#)

[Printer-friendly Version](#)

[Interactive Discussion](#)

**Wavelet Snowmelt
Algorithm over
Antarctica**N. Steiner and
M. Tedesco[Title Page](#)[Abstract](#)[Introduction](#)[Conclusions](#)[References](#)[Tables](#)[Figures](#)[◀](#)[▶](#)[◀](#)[▶](#)[Back](#)[Close](#)[Full Screen / Esc](#)[Printer-friendly Version](#)[Interactive Discussion](#)

All results of the current dynamic algorithm are shown relative to this FT algorithm approach.

We apply these two melt detection algorithms to an enhanced spatial resolution QuikSCAT (Ku band) scatterometer dataset distributed by the Microwave Earth Remote Sensing (MERS) Laboratory with an effective resolution of 5 km gridded to 2.225 km (Early and Long, 2001; Spencer et al., 2003). The enhanced spatial resolution allows for the discrimination melting patterns at sub-ice-shelf resolution and resolves melting patterns and trends that are not apparent in coarse spatial resolution products. High-resolution datasets are ideal for the Antarctic Peninsula, a region of high elevation contrast where the coarse resolution of some microwave observations may underestimate melt due to a large sub-pixel elevation gradient. We focus on melt onset date (MO), melt off date (MF), melt extent (ME) and melt duration (MD) for the whole Antarctic Continent. Results from both CWTM and FT approaches applied to the enhanced resolution QuikSCAT data record are also compared with those obtained from space-borne microwave brightness temperatures from the Special Sensor Microwave/Imager (SSM/I) and melt estimates obtained from the analysis of surface air-temperature values recorded by automated weather stations (AWS). Finally, building on previous studies, the relationships between the melting estimates obtained with the novel method introduced here are discussed in conjunction with time series of the Southern Annular Mode (SAM) index, a major climate driver in Antarctica.

2 Methodology

A general overview of wavelets and the specific methodology applied here is presented in Sect. 2.1. This is followed by a more detailed discussion of the mathematics and examples of wavelet melt-detection in Sect. 2.2. An overview of the processing-steps and operation of the melt-detection algorithm is presented in Sect. 2.3.

2.1 Melt detection using wavelets

The duration of seasonal melting over Antarctica is estimated by means of a wavelet analysis. A wavelet transform unfolds a one-dimensional time-series of σ^0 into a two dimensional power spectrum of position and scale (i.e. inverse-frequency). The wavelet transform can evaluate localized variability of a backscatter time-series at discrete “zooms” through a series of convolutions with a dilating and translating wave-like function (Daubechies, 1992). In this study, we use the wavelet transform as a differential operator, in that it is able to approximate the derivative of a smoothed data series at each time-location. Melting and refreezing events will cause large variations in σ^0 and therefore appear as local maxima or minima in the wavelet transform.

Many studies in the natural sciences have used the wavelet transform to detect changes in one-dimensional time series, for example the detection of tropical convection anomalies (Weng and Lau, 1994) and geomagnetic jerks (Alexandrescu et al., 1995). Wavelet analysis methods have also been applied to snowmelt detection: specifically Liu et al. (2005) apply a wavelet-based methodology to identify large changes in measured brightness temperature values associated with melting events over Antarctica.

We apply an approach similar to Liu et al. (2005), but with several key differences. First, we apply this approach to active microwave (Ku-band, 13.4 GHz) measurements. Additionally, we use no a-priori information, such as statistical or physically based thresholds. Melt and refreezing events are both identified and classified in the framework of singularity detection as introduced Mallet and Hwang (1992). Continuous wavelet transforms are used to detect melting events that appear as discontinuous events in the backscatter time-series and to eliminate those melting events that are determined to be sporadic in time using multi-scale analysis (Mallet and Hwang, 1992; Mallet, 1999; Alexandrescu, 1995). This methodology is novel, and to our knowledge, it is the first time that such approach is applied to remote sensing of snow and ice.

Wavelet Snowmelt Algorithm over Antarctica

N. Steiner and
M. Tedesco

[Title Page](#)

[Abstract](#)

[Introduction](#)

[Conclusions](#)

[References](#)

[Tables](#)

[Figures](#)

◀

▶

◀

▶

[Back](#)

[Close](#)

[Full Screen / Esc](#)

[Printer-friendly Version](#)

[Interactive Discussion](#)



2.2 Continuous wavelet transform and multi-scale analysis

The continuous wavelet transform (CWT) of the seasonal (June of one year through May of the successive year) backscatter, $\sigma^0(t)$ is defined by the convolution product,

$$W\sigma^0(u, s) = \int_{-\infty}^{+\infty} \sigma^0(t) \frac{1}{\sqrt{s}} \psi\left(\frac{t-u}{s}\right) dt = (\psi_s * \sigma^0)(u) \quad (1)$$

- 5 where ψ is the wavelet function, u is the translation parameter, s is the scaling factor and $*$ is the convolution operator (Mallet, 1999). The analyzing wavelet, ψ , is a real-valued, localized zero-mean function with a vanishing integral (e.g., the integral of ψ is zero) (Mallet, 1999; Holschneider, 1995). The analyzing wavelet function used in this study is defined using the first derivative of a Gaussian function (DOG):

$$10 \quad \psi(t) = (-1)^n \frac{d^n \theta(t)}{dt^n} \quad (2)$$

and

$$\theta(t) = \frac{1}{\sqrt{2\pi}} \exp\left(-\frac{t^2}{2}\right) \quad (3)$$

with order, $n = 1$ (Mallet, 1999).

- A wavelet function with a gaussian base is necessary to ensure that wavelet coefficient maxima will be continuous from large to small scales (Mallet, 1999). This allows for the tracing and association of wavelet maxima across scales, a process that is key for multiscale analysis. As an example, a microwave backscattering (σ^0) time series recorded over the Larsen Ice Shelf automated weather station (AWS) during the 2006–2007 season is plotted in Fig. 1a, with the corresponding CWT plotted in Fig. 1b. The magnitude of local maxima or minima in $W\sigma^0$ (black and white areas respectively) are

TCD

7, 2635–2678, 2013

Wavelet Snowmelt Algorithm over Antarctica

N. Steiner and
M. Tedesco

Title Page

Abstract

Introduction

Conclusions

References

Tables

Figures

◀

▶

◀

▶

Back

Close

Full Screen / Esc

Printer-friendly Version

Interactive Discussion



Wavelet Snowmelt Algorithm over Antarctica

N. Steiner and
M. Tedesco

[Title Page](#)

[Abstract](#) [Introduction](#)

[Conclusions](#) [References](#)

[Tables](#) [Figures](#)

[◀](#) [▶](#)

[◀](#) [▶](#)

[Back](#) [Close](#)

[Full Screen / Esc](#)

[Printer-friendly Version](#)

[Interactive Discussion](#)



correlated with the magnitude of backscatter change (Liu et al., 2006). This is expected as ψ is equivalent to the first derivative of a smoothing function as indicated in Eqs. (2) and (3). In Fig. 1b conical field of negative $W\sigma^0$ intercepts the scale-axis at its narrowest width at a position ($u = 185$) coincident to a ~ 20 dB decrease in σ^0 over several days. Fields of elevated $W\sigma^0$ in a CWT, or “cones of influence” (Mallet, 1999), are located where the data in the time-series (or its derivative) behave as a discontinuous function (Mallet and Hwang, 1992; Holschneider, 1995; Mallet, 1999). Melting or re-freezing events create, therefore, cones of influences that will converge at fine scales to the position of signal discontinuity (Mallat and Hwang, 1992; Mallet, 1999; Lui et al., 2006). We refer to these positions as singularities (e.g. Mallet and Hwang, 1992).

The values contained in a cone of influence compose the scalar components (the signal change relative to the temporal scale) of that transition and are used in multi-scale analysis. We define the set of all CWT coefficient maxima along the “ridge” of the maxima cone as the wavelet transform modulus maxima line (WTMML) for each singularity. These positions are found where $(\delta/\delta t)W\sigma^0(u, s) = 0$ and are connected across adjacent scales from large duration to small (Hermann, 2001; Mallet, 1999; Mallet and Hwang, 1992; Alexandrescu, 1995). The CWT, although redundant in its frequency or scale representation of any signal, is necessary in this application as these positions are not easily connected if determined only at discrete dyadic scales (e.g., Liu et al., 2006). Additionally, tracing CWT maxima to the finest temporal scale ensures the accurate localization of melting events as these positions are shifted with increasing scale as evident in Fig. 1b.

The WTMML is then used to characterize the nature of σ^0 change at each singularity using multiscale analysis (e.g. Mallet and Zhong, 1992; Le Gondic et al., 2002). The WTMML for several singularities in σ^0 are highlighted in Fig. 1b and are labelled 1 through 4. The apparent regularity of a σ^0 time-series in the immediate neighbourhood of each singularity can be estimated from the wavelet coefficient values that compose each WTMML (e.g. Mallet, 1999). The Holder exponent, a , is a measure of estimated regularity at the terminating position of each WTMML (Mallet and Zhong, 1992). An

estimate of a is found as (Mallet, 1999):

$$|W\sigma^0(u,s)| \leq Ae^a \quad (4)$$

so that

$$\ln |W\sigma^0(u,s)| \leq a \ln a + \ln A \quad (5)$$

- 5 Here, $|W\sigma^0|$ correspond to the maximum wavelet coefficients that compose the WT-MML. Using Eqs. (4) and (5), a , as well as the coefficient A are determined using a linear least-squares regression.

Each WTMM can be then classified by a using several theoretical transition types whose a value is known. For example, a step-like, or Heaviside function, will result in 10 a equal to 0 (Le Gonidec et al., 2003), a ramp-like or smoothed transition has a of 1 or greater (Mallet, 1999; Le Gonidec et al., 2003). For wet snow detection, we assume melt onset transitions (e.g., similar to $u = 185$ in Fig. 1b) can be approximated by either a step-like or smoothed transition. Here the corresponding value of a is $a_1 = 0.27$. Due to the complex nature of a time series, a values determined by Eq. (5) are not expected 15 to match the theoretical case since nearby singularities will have contributions to the WTMM (i.e. cones of influence will overlap if transitions are close in time) (Mallet, 2001). In Fig. 1a we observe a more gradual (smoothed) σ^0 transition, coincident with a refreezing event, near $u = 250$ where the determined regularity ($a_2 = 0.4$, Fig. 3c).

Spike-like or cusp-like transitions will produce negative a in multi-scale analysis (Le 20 Gonidec et al., 2003; Mallet, 1999). In Fig. 1a, a σ^0 fluctuation, corresponding to position $u = 140$ in Fig. 1b illustrates a transition that is sporadic in time. This transition produces two WTMM, shown in Fig. 1d, labelled 3 and 4, having negative and positive $W\sigma^0$ components, respectively. From Eq. (2) it is determined that both can be approximated with negative a values ($a_3 = \sim -0.27$, $a_4 = \sim -0.4$). Negative a values associated 25 with a WTMM indicate the signal is both discontinuous and non-differentiable at that position, here $u = 140$ (Mallet and Hwang, 1999). In terms of melt detection, by removing all negative a transitions, we eliminate sporadic σ^0 changes that return to “dry”

Wavelet Snowmelt
Algorithm over
Antarctica

N. Steiner and
M. Tedesco

[Title Page](#)

[Abstract](#)

[Introduction](#)

[Conclusions](#)

[References](#)

[Tables](#)

[Figures](#)

◀

▶

[Back](#)

[Close](#)

[Full Screen / Esc](#)

[Printer-friendly Version](#)

[Interactive Discussion](#)

conditions rapidly relative to the reference scale. This creates a melt detection process that eliminates sporadic melting events.

For locations that do not experience melting events, changes in backscatter associated with snow properties changes are of low magnitude compared to changes in liquid water content (LWC), but produce positive a in multi-scale analysis. To reduce the influence of falsely classified melting events, we set a minimum threshold for $|W\sigma^0|$, at each temporal scale along the WTMML, corresponding to one order of magnitude (10 \times) greater than that observed during winter (June, July and August months). This is a conservative threshold and this choice does not appear to influence classification for areas experiencing melt.

2.3 Melt detection process

From all wavelet transform modulus maximum lines (WTMML) for each backscattering time series, individual WTMML are evaluated as a possible melting event according to the following criteria:

1. The WTMML must have a scale component that extends above a set minimum scale. Signal noise, and noisy transition in backscatter produce WTMML only at small scales (i.e. high frequency). We set the minimum scale at 2⁵. We observed that using a scale of 2³ similar to Liu et al. (2005) could not eliminate all noisy transitions during the melting season. This increased minimum scale relative to previous studies is expected since the enhanced resolution remote sensing product used in this study is more noisy than the coarser resolution one (Ashcraft and Long, 2003; Spencer et al., 2003).
2. All $|Wf|$ along the WTMML must have a value one order of magnitude (10 \times) greater than those measured during the winter season. For areas experiencing melt, this condition does not have a large effect since $|Wf|$ produced at all scales for a ~ 3 dB transition in backscatter is many orders of magnitude greater than observed wintertime conditions. However, areas that experience snow property

TCD

7, 2635–2678, 2013

Wavelet Snowmelt Algorithm over Antarctica

N. Steiner and
M. Tedesco

Title Page	
Abstract	Introduction
Conclusions	References
Tables	Figures
◀	▶
◀	▶
Back	Close
Full Screen / Esc	
Printer-friendly Version	
Interactive Discussion	

changes, but no seasonal melt, will produce WTMM with large scalar components since these changes are not “noisy” transitions and are temporally sustained. Since changes in LWC produce greater differences in backscattering values compared to snow property changes over a relatively short period (Stiles and Ulaby, 1980), we threshold the $|Wf|$ values of a WTMM, at all spatial scales, with a value an order of magnitude ($10\times$) greater than observed wintertime conditions.

5

3. The Holder exponent, a , of each WTMM must be equal to or greater than zero. For reasons discussed in the previous section, we eliminate spike-like transitions in backscatter using a test of point-wise signal regularity.
- 10 All signal transitions that meet the three criteria above are considered to be either melt onset or refreeze events. To define periods of melt we select the WTMM that extends to the largest scales that has the greatest mean $|Wf|$. This transition is matched with a WTMM greatest mean $|Wf|$ in the set of transitions of opposite magnitude. This defines one seasonal melting event. We assume that refreeze must follow melting.
- 15 This process is repeated with the remaining melt-related WTMM to define additional periods of melting or periods of sustained re-freeze within melting. The melt onset (MO) is defined as the first day of melting, and melt off (MF) is defined as the last melting day plus one. The melting duration (MD) at any pixel location is the total number of days when melting occurs.
- 20 To create a dataset for comparison, a fixed threshold melting record is created from the QuikSCAT backscatter. Melting where $\sigma^0(t)$ is at or below 3 dB minus winter (JJA) mean backscatter, equivalent to the expected loss from a 2.8 cm layer of 1 % volumetric water content as in Ashcraft and Long (2006). Melting events whose durations are shorter than 3 continuous days are removed from the melting record at each pixel
- 25 (Nghiem et al., 2007; Tedesco and Monaghan, 2009).

For our study, we use a MATLAB® wavelet analysis software library (WaveLab 850) distributed by Stanford University and available at www-stat.stanford.edu/~wavelab/. Because of the computationally intensive nature of the problem and of the high number

TCD

7, 2635–2678, 2013

Wavelet Snowmelt Algorithm over Antarctica

N. Steiner and
M. Tedesco

Title Page

Abstract

Introduction

Conclusions

References

Tables

Figures

◀

▶

Back

Close

Full Screen / Esc

Printer-friendly Version

Interactive Discussion



of pixels necessary to cover the entire Antarctica continent at the spatial resolution considered here (2.225 km), we also made use of the MATLAB's parallel computing toolbox, running on a dedicated server using 8 processing-cores. In this configuration, one continent-scale melting-season requires between 24 and 48 h of processing.

5 3 Datasets

3.1 SeaWinds on QuikSCAT

Enhanced spatial resolution melting maps (gridded at 2.225 km) are derived from the enhanced resolution SeaWinds (commonly referred to by the satellite name, QuikSCAT) scatterometer dataset distributed by the Microwave Earth Remote Sensing (MERS) Laboratory at Brigham Young University (BYU, <http://www.mers.byu.edu/>). The SeaWinds instrument is a conically scanning pencil-beam width scatterometer that records normalized radar cross-section measurements in the Ku band (13.4 GHz). This instrument records both horizontal and vertical polarizations at a fixed incidence angle of 46° for horizontal polarizations and 54.1° for vertical polarizations (Long and Hicks, 2000). The effective $\sim 7 \times 30$ km instantaneous field of view of the QuikSCAT range-Doppler processed “slice” product (Spencer et al., 2003) is enhanced through a scatterometer image reconstruction algorithm (SIR) developed at BYU. By combining multiple observations that are weighed within with the sensor's antenna function, the SIR algorithm can recover information attenuated at the antenna side-lobe, and thereby effectively increasing the spatial resolution of the standard scatterometer product (Early and Long, 2001). This resolution enhancement is done at the expense of increased signal noise. In view of the strong change in measured backscatter following snow-melt, the increase in signal noise does not affect melt detection considerably, hence allowing for the generation of a surface melting product at a gridded spatial resolution of 2.225 km (Trusel et al., 2012; Barrand et al., 2013). In addition, the CWT method is well suited for noisy datasets since high frequency, noisy transitions in backscatter are

TCD

7, 2635–2678, 2013

Wavelet Snowmelt Algorithm over Antarctica

N. Steiner and
M. Tedesco

Title Page

Abstract

Introduction

Conclusions

References

Tables

Figures

◀

▶

Back

Close

Full Screen / Esc

Printer-friendly Version

Interactive Discussion



not likely to create WTMMs that extends to large scales (e.g., Liu et al., 2006) and those that do will decrease in $|Wf|$ with increasing scale, leading to negative Holder exponents (a) and will subsequently be removed in the melt-detection methodology.

3.2 Automated weather stations

- 5 Automated weather station data from the Antarctic Meteorological Research Center (AMRC) and Automatic Weather Station program, maintained by the Space Science and Engineering Center at the University of Wisconsin, Madison (AMRC, SSEC, UW-Madison), is used to evaluate the results of the melt detection algorithms. For our comparison, we use the hand corrected 3-hourly air temperature records. The AWS used
10 in this study are: Larsen Ice Shelf (Lat: 67.01° S Long: 61.55° W Elev: 17 m), Uranus Glacier (Lat: 71.43° S Long: 68.93° W Elev: 780 m), Fossil Bluff (Lat: 71.33° S Long: 68.28° W Elev: 63 m), Butler Island (Lat: 72.21° S Long: 60.17° W Elev: 91 m), Pegasus South (Lat: 77.99° S Long: 166.57° E Elev: 5 m), and Limbert (Lat: 75.91° S Long: 59.26° W Elev: 40 m). For each AWS, air-temperature measurements and backscatter
15 are spatially and temporally co-registered using overpass times available from MERS-SCP. Melting is determined from AWS air-temperature measurements where there is at least 2–3 h daily above-zero measurements. For Antarctica, extreme fluctuations in daily temperature often prevent the daily mean temperature from exceeding 0 °C, though satellites observations indicate that melting is likely taking place. A threshold
20 below 0 °C is often used to account for this fact (Tedesco and Monaghan, 2009; van den Broeke et al., 2010), or in those cases where additional measurements are available, such as surface short-wave and long-wave radiative fluxes, melting may be determined using a simple thermodynamic models (van den Broeke, 2005). From the lack of a defined sub-zero threshold for each AWS station, as well as of sufficient surface measurements for modeling approaches, we choose a temporal threshold at least
25 6 h of above zero measurements in one day to establish melting conditions from AWS measurements. This is equivalent to at least 2 daily above zero measurements for the 3 h AWS air temperature dataset. Once melt is estimated from AWS data, we study

TCD

7, 2635–2678, 2013

Wavelet Snowmelt Algorithm over Antarctica

N. Steiner and
M. Tedesco

Title Page	
Abstract	Introduction
Conclusions	References
Tables	Figures
	
Back	Close
Full Screen / Esc	
Printer-friendly Version	
Interactive Discussion	

Title Page

Abstract

Introduction

Conclusions

References

Tables

Figures

◀

▶

◀

▶

Back

Close

Full Screen / Esc

Printer-friendly Version

Interactive Discussion



the number of days when the remote sensing- and air temperature-based estimates agree (true-positive), the omission error, computed as the percentage of days when air-temperature indicates melting but the remote sensing-based approach does not (true-negative), and the commission, computed as the percentage of days when the satellite data indicates melting but this is not occurring from the analysis of air temperature (false-positive).

4 Results and discussion

Figure 2a and b show maps of mean (2000 through 2009) seasonal melt duration (MD), defined as the number of days per year where melting is detected, obtained with the fixed threshold method (FT3), and with the dynamic wavelet-based method (CWT) respectively. Figure 2c shows the map of the difference between MD obtained with the two methods ($\Delta\text{MD} = \text{MD}_{\text{FT3}} - \text{MD}_{\text{CWT}}$). Although the spatial patterns of MD from the two methods are similar, systematic differences exists regionally and with elevation change. For example, the CWT based method shows a strong regional underestimation of MD over areas of the Antarctic Peninsula and a overestimation of MD over for much of the Dronning Maude Land with respect to a FT3 approach. There is also a clear transition along the Antarctic Peninsula from positive to negative ΔMD from lower to higher elevations.

For all areas and years, the CWT algorithm produces an average MD value of 28 days, versus 41 days obtained with the FT3 algorithm. The mean continent-scale melt index (MI), defined as the area subject to melting times the number of melting days, obtained with the CWT approach is $2.971 \times 10^7 \text{ day km}^2$, a value greater than the of $2.813 \times 10^7 \text{ day km}^2$ obtained with the FT3 approach. When considering only melt extent (ME), the CWT algorithm estimates that 6.23 % of the total surface area of Antarctica is subject to at least one day of melting per season compared to the 8.14 % found using the FT3 method. This implies that the CWT method estimates longer mean melting durations over smaller areas compared to the FT3 approach.

Wavelet Snowmelt Algorithm over Antarctica

N. Steiner and
M. Tedesco

At continental scale, the average melt onset day (MO), expressed as day of the year, determined by the CWT approach is day 347 (e.g., 13 December for non-leap years) and in the case of the FT3 algorithm is day 352. The mean melt off date (MF) date for the whole of Antarctica between methods differs by 6 days, with the FT3 suggesting a later refreezing (day 28) than the CWT approach (day 22). The difference (5 days MO and 6 days MF) between the seasonal MO and MF obtained with the two approaches is small compared to the standard deviation (σ) of either method, being $\sigma_{\text{FT3}} = 26$ days and $\sigma_{\text{CWT}} = 16$ days for MO and $\sigma_{\text{FT3}} = 28$ days and $\sigma_{\text{CWT}} = 17$ in MF over all locations and years.

The maximum ΔMD between the FT3 and CWT method (Fig. 2c) is observed over areas of east Antarctica near the Donning Maud Land. Here ΔMD averages 25 days. This difference can be attributed to both differences in the in mean season length (defined as the continuous period between MO and MF) and the time that melting is sustained through a season. Differences in mean seasonal length accounts for only ~14 % of the observed ΔMD found between methods. In light of similar melting season lengths, it is apparent that a majority of ΔMD can be attributed to how melting is sustained through the melting season. By comparing the percentage of melt days per melting season length (calculated as $(\text{MF}-\text{MO})/\text{MD}$), we find that the FT3 method detects melt for 65 % of the melting season while the CWT approach detects melt for 95 % of the melting season. This important difference, as illustrated in more detail in the following, can be partly attributed to threshold values that may underestimate the actual backscattering response to increasing liquid water content and where actual backscatter changes are close to seasonal in backscatter threshold (e.g. 3 dB). With signal noise, a fixed threshold algorithm will alternate between classifications of melting and refreeze as backscatter fluctuates around the backscatter threshold. Alternatively, fluctuations in backscatter can also be attributed to rapid melt-refreeze events in areas where the liquid water content is not sustained through diurnal refreeze cycles. These cases are difficult to validate without further information and are a weakness of fixed threshold algorithms in varying snow property and temperature regimes. For the

[Title Page](#)

[Abstract](#) [Introduction](#)

[Conclusions](#) [References](#)

[Tables](#) [Figures](#)

◀

▶

◀

▶

[Back](#) [Close](#)

[Full Screen / Esc](#)

[Printer-friendly Version](#)

[Interactive Discussion](#)

Wavelet Snowmelt Algorithm over Antarctica

N. Steiner and
M. Tedesco

[Title Page](#)

[Abstract](#) [Introduction](#)

[Conclusions](#) [References](#)

[Tables](#) [Figures](#)



[Back](#) [Close](#)

[Full Screen / Esc](#)

[Printer-friendly Version](#)

[Interactive Discussion](#)

for less than 1 % of all detected melting events (Fig. 3b). The inclusion of short-duration melting events using a fixed threshold leads to an overall decreased overall mean MD value. A majority (> 50 %) of MD for the FT3 method are under 27 days, compared to a 37 MD for the CWT method. Both methods show better agreement for longer duration 5 MD, where about 20 % of all MD for both methods are 60 days or longer.

An analysis of selected backscattering time-series during the melting season along with regionally integrated melting is presented to show difference between the CWT and FT3 algorithms. Two regions of Antarctica, namely the Antarctic Peninsula and the coastal area of the Dronning Maude Land, are shown in Fig. 4. These regions 10 are chosen because they exhibit the largest differences in regionally integrated Δ MD between algorithms. For the Antarctic Peninsula during the 2004–2005 melting season, FT3 values (Fig. 4a, solid gray line) exhibit an early season (November 2004) peak in ME reaching an extent of up to ~ 80 % of the yearly maximum for a period of ~ 8 days. This transient melting event is not observed in the time-series of melting extent from 15 the CWT approach as melt (Fig. 4a, dotted black line). A time series of backscatter from within the region and over this same period is shown in Fig. 4c. As indicated by a shaded region for the CWT method, and by the location of the 3 dB threshold for the FT3 approach in Fig. 4c, we observe that the CWT excludes several melting events at the beginning of the season (outside of the shaded area) that correspond to the large 20 increase in region-wide melting extent as shown by the FT3 (Fig. 4a). It is apparent that this omission by the CWT at this location is representative of the differences in melting extent observed regionally. Much of difference between methods over the Peninsula can be attributed to non-sustained short-term melting/refreezing events, as shown in Fig. 4a, before and after the period when the majority of melting occurs. Additionally, it 25 is clear that the MO date for a majority of the Antarctic Peninsula determined using the FT3 approach (defined as the first melting event greater than 3 days) will correspond to the brief November melting event that, as shown in Fig. 4a, may be several weeks prior to the main melting events.

Wavelet Snowmelt Algorithm over Antarctica

N. Steiner and
M. Tedesco

Title Page

Abstract

Introduction

Conclusions

References

Tables

Figures

◀

▶

◀

▶

Back

Close

Full Screen / Esc

Printer-friendly Version

Interactive Discussion

Time-series of ME and σ^0 for the Dronning Maude Land are shown in Fig. 4b and d. For this year over the Dronning Maude Land, the CWT method finds a greater regionally integrated MI with respect to the FT3 method. A time-series of σ^0 chosen from within the Dronning Maude Land, as in Fig. 4d, shows that the FT3 method will classify multiple melt/refreeze events as σ^0 changes rapidly around the threshold value while the CWT will record a single melting event. This will lead to estimates of a shorter melt duration by the FT3. From inspection of results it is found that this is representative of the majority of the cases where the CWT finds greater melting durations than the FT3. Additionally, melting events as shown in Fig. 4d will not create a considerable difference in MO or MF dates.

An estimate of the average length of MD omitted by the CWT (i.e. the minimum number of days where the CWT will detect melting) is determined empirically from melting records over the Antarctic Peninsula. Figure 5 shows the cumulative sum (lines) and histogram (bars) of the length of melting days obtained from the two approaches over the Antarctic Peninsula for two selected years of 2003–2004 and 2005–2006; these seasons are selected as an example of a relatively low and high mean melting index respectively. It is important to note that this is not an analysis of total MD per season, as shown in Fig. 3, but rather the length of a period during the melting season where FT3 detects any melting event and CWT does not. During the 2003–2004 season, ~ 60 % of MD values differ by only 1 day, ~ 20 % show differences of two days, with the remaining values differing by more than 6 days (~ 90 % of observations are 6 days or less). This 6 day duration is similar to the temporal filtering methods used in previous melting studies to eliminate transient melting events (e.g., 3 days, Nghiem et al., 2001; Tedesco, 2009).

Figure 6 shows results concerning the difference between the outputs of the two approaches as a function of elevation for the AP, the Dronning Maude Land and the whole of Antarctica. For the Dronning Maud Land region, the melt index difference between the two methods ($\Delta MI = MI_{FT3} - MI_{CWT}$) is negative, independent of elevation. For the AP however, the mean difference between methods is positive, and will vary

Wavelet Snowmelt Algorithm over Antarctica

N. Steiner and
M. Tedesco

[Title Page](#)

[Abstract](#)

[Introduction](#)

[Conclusions](#)

[References](#)

[Tables](#)

[Figures](#)

◀

▶

◀

▶

[Back](#)

[Close](#)

[Full Screen / Esc](#)

[Printer-friendly Version](#)

[Interactive Discussion](#)

[Title Page](#)

[Abstract](#)

[Introduction](#)

[Conclusions](#)

[References](#)

[Tables](#)

[Figures](#)

◀

▶

[Back](#)

[Close](#)

[Full Screen / Esc](#)

[Printer-friendly Version](#)

[Interactive Discussion](#)



with elevation. For areas below 400 m a.s.l. the CWT method underestimates MI with respect to the FT3 method. Conversely, above 400 m a.s.l., the MI difference becomes negative. Building on our previous analysis in this paper, we infer that for the Antarctic Peninsula at lower elevations, we find that the melt difference is due to the omission of short-duration melting events while at higher elevations we find that melt-detection differences are more closely related to short melt-refreeze cycles at high elevations and a lesser backscatter response to snow-wetness. This may indicate the need for terrain correction when using fixed-threshold methods.

4.1 Comparison between QuikSCAT-derived melting and analysis of automated weather stations

Results of the FT3 and CWT approaches are compared with estimates of melting derived from surface air temperatures measured by AWS. Because of the lack of in-situ liquid water content or snow temperature measurements, melt is estimated from AWS air temperatures where the temperature is above zeros for at least 6 h per day. The time series of co-registered backscattering, air temperature and positive temperatures for the stations considered in this study are plotted in Fig. 7. We evaluate the accuracy, commission, and omission in percentage at each station and the results are presented in Table 1. Accuracy is defined as the percentage of cases where surface temperature and spaceborne-based estimates both detect melting. Commission is defined as the percentage of cases when remote sensing algorithms indicates melting but AWS does not. Lastly, omission indicates the percentage of cases when AWS suggests melting but the remote sensing algorithms do not.

For stations that experience at least 10 days of melt per year (Butler Island (BI), Fossil Bluff (FB) and Larsen Ice Shelf (LS) stations), we find the highest rates of agreement. For these stations the FT3 approach performs with more accuracy (~ 10 %) than the CWT approach. The LS and FB stations show the highest overall agreement, averaging 87 % (77 %) and 75 % (66 %) for the FT3 (CWT) approach for all years. The LS and FB stations have large magnitude and sustained change in backscatter over the

**Wavelet Snowmelt
Algorithm over
Antarctica**N. Steiner and
M. Tedesco[Title Page](#)[Abstract](#)[Introduction](#)[Conclusions](#)[References](#)[Tables](#)[Figures](#)[◀](#)[▶](#)[Back](#)[Close](#)[Full Screen / Esc](#)[Printer-friendly Version](#)[Interactive Discussion](#)

melting season (Fig. 7a and b). For the Limbert (LI), BI and Uranus Glacier (UG) stations, shown in Fig. 7c–e respectively, the difference in accuracy for the FT3 and CWT methods is greater, up to 43 % (FT3 > CWT) between methods. At these stations, the majority of melting occurs as short duration events. This is not the case during the 2002–2003 and 2003–2004 seasons for the LI and UG respectively, where the backscattering time-series shows a substantial decrease in backscatter. In this case both remote sensing methods are in good agreement with AWS estimates. Figure 7a and Fig. 7b show that a majority of the difference between methods at these stations occur during transitional periods, meaning near the seasonal MO or MF. For the Pegasus South (PS) station, the CWT method is in better agreement with AWS compared to FT3 with a 10 % greater mean accuracy. At the PS station the apparent backscatter response to melting, as shown in Fig. 7f, is below detection by the FT3. Additionally, PS station has the highest mean air temperature during melting conditions among these stations at +2.16 °C and a mean loss of +1.86 dB (from winter mean) during AWS defined melting. Only the UG station has a smaller backscatter change, of +1.80 dB with an average temperature of +0.79 °C during melting. In contrast, the Larsen Ice Shelf averages a loss of +15.07 dB with mean temperature of +1.06 °C during AWS defined melting.

Omission errors for all stations show an average of 12 % fewer false positives for the FT3 compared to the CWT. For the LI AWS shown in Fig. 7e the CWT method has a maximum mean omission error of 83 %, compared to the FT3 at 40 %. The LI station has a short melting season, averaging close to 4 days/yr in length from AWS derived melting. A majority of these melting events are omitted using the CWT. Conversely, the FT3 approach detects these events with relatively high accuracy (83 %). These findings are constant with the basis of the CWT algorithm, which aims to detect only sustained melting events. For the LS, we find the lowest rate of omission, averaging 34 % (25 %) for the CWT (FT3). Commission errors are found to be small for both methods, averaging 3 % for all stations for both the FT3 and CWT respectively.

4.2 Comparison with results from passive microwave measurements

We compare melting records from passive microwave Special Sensor Microwave Imager (SSM/I) observations using approaches proposed in the literature with the outputs of both the CWT and FT3 methods. The SSM/I derived melting is produced using two

5 methods. The first is an FT approach as in Zwally and Fiegles (1994), here denoted as M+30K. The second dataset is produced using a dynamic electromagnetic modelling based detection approach as in Tedesco (2009), here denoted as MT09. Outputs from both methods are projected onto the 2.225 km QuikSCAT grid using nearest-neighbour interpolation.

10 The values of seasonal integrated MI for Antarctica for both active and passive MW methods are plotted in Fig. 8a. The M +30 K and CWT approaches show the most similar magnitude in seasonal MI, where the relative difference (defined as $|MI_1 - MI_2| / \frac{1}{2}(MI_1 + MI_2)$) is 9 %. This is only 2 % greater than the difference between the CWT and FT3 methods (7 %). There is a slightly greater relative difference between the FT3 and M+30K of 11 %. The MT09 method finds on average, a 40 % greater MI than the FT3 method, and 35 % greater than the CWT.

15 For individual seasons, all methods find a MI maximum during 2004–2005. The active and passive methods, however, do not agree on the year of minimum MI. Indeed, both the CWT and FT3 approaches find a minimum MI during the 1999–2000 seasons while the passive methods find a minimum during the 2008–2009 melting season where a majority of this difference is from the Antarctic Peninsula. Melting index derived using the M +30 K and the CWT methods are highly correlated ($r = 0.943$ and $p < 0.01$), with a MI root mean squared error (RMSE) of 2.74×10^6 day km 2 . A comparison between the FT3 and M + 30 K approaches yields a correlation of $r = 0.922$ with $p = 0.001$, and a RMSE close to 3.10×10^6 day km 2 as shown in Fig. 8b.

20 A comparison between active datasets (FT3 and CWT) and the MT09 passive microwave dataset also shows a high degree of correlation. The MT09 when compared to the FT3 has a correlation with Pearson's coefficient of $r = 0.931$ with $p < 0.001$ and

TCD

7, 2635–2678, 2013

Wavelet Snowmelt Algorithm over Antarctica

N. Steiner and
M. Tedesco

[Title Page](#)

[Abstract](#)

[Introduction](#)

[Conclusions](#)

[References](#)

[Tables](#)

[Figures](#)

◀

▶

◀

▶

[Back](#)

[Close](#)

[Full Screen / Esc](#)

[Printer-friendly Version](#)

[Interactive Discussion](#)



a RMSE of 2.48×10^6 day km 2 . In comparison with the FT3, the MT09 has a Pearson's coefficient of $r = 0.911$ ($p = 0.002$) with a RMSE = 2.91×10^6 day km 2 . For both PMW methods there is both a greater degree of correlation and a lower RMSE for the CWT as compared to the FT3.

The spatial differences between the mean MD estimated using the M+30K approach and the CWT, shown in Fig. 9a, and the FT3, as shown in Fig. 9b, reveals patterns in the magnitude of difference between methods ($\Delta\text{MD}_{\text{FT3}} = \text{M} + 30\text{ K} - \text{FT3}$). Over large ice-shelves (e.g. the Larsen, and Amery Ice Shelves), $\Delta\text{MD}_{\text{FT3}}$ is close to +10 days, Fig. 9a. Over the same regions, $\Delta\text{MD}_{\text{CWT}}$ between the M + 30 K and the CWT algorithms difference is $\sim +20$ days, Fig. 9b. The tendency for the PMW data to overestimate AMW estimates (close to +10 or +20 ΔMD in most cases) is usually bordered, to some degree, by an area of underestimation by the PMW measurements. A majority of areas that exhibit melting in Antarctica generally occurs at ice-ocean boundaries. For the Antarctic Peninsula (among other places) areas of melt occur adjacent to sharp contrasts in elevation. For many of these areas sub-pixel mixing will likely lead to a decrease in the observed brightness temperatures of some melting areas. For example, over the coastal regions of the Dronning Maude Land we find the systematic occurrence positive ΔMD bordered negative ΔMD . These negative ΔMD are found adjacent to ocean pixels and high elevations, and such are likely due to a sub-pixel mixing effect. In another case, the relatively narrow King George VI (lat: -71.965 , lon: -67.807) ice shelf, located roughly east of Wilkens Ice Shelf (lat: -67.525 , lon: -62.775), appears to increase the apparent MD of the surrounding high elevation areas for the PMW case, resulting in a large positive ΔMD . Since mixed pixel effects dominate the spatial differences between methods, it is difficult to determine a relationship between MD methods over similar areas other than the positive ~ 10 days (FT3) and ~ 20 days (CWT) reported previously.

An analysis of correlation between co-located melting durations from active microwave datasets and the M + 30 K method indicates that the FT3 has a higher degree of correlation with the passive microwave M + 30 K method, with $r = 0.782$ ($p < 0.001$),

Wavelet Snowmelt Algorithm over Antarctica

N. Steiner and
M. Tedesco

[Title Page](#)

[Abstract](#) [Introduction](#)

[Conclusions](#) [References](#)

[Tables](#) [Figures](#)

[◀](#) [▶](#)

[◀](#) [▶](#)

[Back](#) [Close](#)

[Full Screen / Esc](#)

[Printer-friendly Version](#)

[Interactive Discussion](#)



Fig. 9c. The CWT method has a Pearson's coefficient of $r = 0.665$ ($p < 0.001$) with the M + 30 K, Fig. 9d. Both AMW methods find a RMSE of close to 14 days in comparison with the M + 30 K. A first order least squares regression between CWT and M + 30 K shows a 13 day positive bias, whereas for the FT3 method a positive 3 day bias is found. Artefacts visible in the scatterplot, as shown in Fig. 9c and d, appear as vertical stripes of data points indicate a high degree of variability for many pixels with similar MD as detected using the M + 30 K. These artefacts are likely due to the difference in spatial resolution, and a result of a high degree of sub-pixel variability as previously discussed. From visual interpretation of in Fig. 9c and d we can see a larger component of the melt dataset for the FT3 method falls along the 1 : 1 line. For the CWT method, points appear to underestimate MD as compared to M + 30 K, or vice versa. It also appears that the CWT method finds greater MD for shorter durations, evident by a cluster of points 0 to 50 MD for CWT and 0 to 20 days for M + 30 K. This relationship is similar to observation between AMW methods. The relatively strong agreement between AMW and PMW integrated melting extent, shown in Fig. 8a, indicates that the high sub-pixel variability is averaged-out when integrated over the entire dataset.

4.3 Antarctic melting and the Southern Antarctic Mode

The Southern Hemisphere Annual Mode (SAM) Index is a measure of the atmospheric pressure gradient between the middle and high latitudes (Thompson and Wallace, 2000). Here, the SAM index is defined by the mean monthly zonal sea level pressure difference between the 40° and 65° south latitude as in Marshall (2003). A positive SAM index generally coincides with lower than normal near surface temperatures for Antarctica, leading to a continent scale negative correlation between SAM indexes and melting over Antarctica (Tedesco and Monaghan, 2009). Positive SAM conditions have been linked to an increase in the westerly flow over the AP, due to the development of a consistent low pressure area to the east of the AP (Marshall et al., 2011). This low pressure system causes an increase in the advection of warmer air to the western edge of the Antarctic Peninsula. In some cases this warmer air will flow over the topographic

Wavelet Snowmelt Algorithm over Antarctica

N. Steiner and
M. Tedesco

[Title Page](#)

[Abstract](#)

[Introduction](#)

[Conclusions](#)

[References](#)

[Tables](#)

[Figures](#)

[◀](#)

[▶](#)

[Back](#)

[Close](#)

[Full Screen / Esc](#)

[Printer-friendly Version](#)

[Interactive Discussion](#)

Title Page

Abstract Introduction

Conclusions References

Tables Figures

◀ ▶

◀ ▶

Back Close

Full Screen / Esc

Printer-friendly Version

Interactive Discussion



barrier of the Antarctic Peninsula (overflow conditions) to areas of the eastern Antarctic Peninsula (Van Lipzig et al., 2008). This process is assumed to increase the magnitude of melting for the Eastern Antarctic Peninsula through the warmer advected air and wind-driven melting (Marshall, et al., 2011).

Over the Antarctic Peninsula, Tedesco and Monaghan (2009) find a weak negative correlation between regionally averaged melting for the AP and SAM conditions. From correlations found using the QuikSCAT AMW dataset and SAM on a per-pixel basis (not regionally averaged) we find that correlation with SAM is spatially variable, as shown in Fig. 10. For the western and eastern AP ice shelves we find a moderate, positive, correlation with SAM for both the CWT and FTW methods. At higher elevations we find a moderately negative correlation with SAM that is most apparent using threshold-based methods for melt detection. For the eastern AP, the CWT method finds a strong positive correlation with SAM conditions over eastern portions of the Larsen C Ice Shelf, while the FT3 does not. In terms of the melting season, it is found that there is also a moderate, but not statistically significant at a 95 % confidence level, correlation with early MO detected by the CWT method (averaged over the AP) and positive SAM ($r = 0.57, p = 0.09$). This is not the case with the FT3 method ($r = 0.05, p = 0.15$). This indicates that positive SAM conditions may be related an earlier onset in persistent melting for portions of the Eastern Antarctic Peninsula.

20 5 Summary and conclusion

The use of a combined continuous wavelet transform and multi-scale analysis (CWT) is able to detect changes in the backscattering signal upon an increase in LWC. This methodology does not require an estimation of the expected response to snow-melt and is therefore applicable to spatially variable snow characteristics as well and is applicable across instrumentation. Estimated mean MD derived from the CWT and a more standard fixed threshold method are well very correlated, $r = 0.897$ ($p < 0.001$) with a root mean squared error (RMSE) of ~ 9 days. However, for the average melt duration,

Title Page

Abstract Introduction

Conclusions References

Tables Figures

◀

▶

◀

▶

Back Close

Full Screen / Esc

Printer-friendly Version

Interactive Discussion



we found that there is as a 19 % difference in absolute MD, where the CWT method averages 13 days longer MD in comparison. This is largely due to the omission of shorter duration refreeze events, most of which are 6 days or less, by the CWT in areas where there is a backscatter response close to the threshold value set by the FT3. Alternately,

for areas of the Antarctic Peninsula, shorter duration melting events during transitional periods are omitted by the CWT. In terms of melting onset/refreeze timings, it is found that the mean melting season length (MF-MO), estimated in both methodologies also agrees within 2 days.

From evaluation of melting over the Antarctic Peninsula for both methodologies, we found that the average MD difference is less than at the continent scale, having a 5 day greater MD found by the CWT method. When observing the season length, there is an apparent early melt onset detected by the FT3 method, 12 days before the CWT. This earlier seasonal melt onset most likely caused by small duration early season melting events, as illustrated during the 2004–2005 season, where the melt index reaches ~ 80 % of its maximum seasonal value for close to 8 days. It is shown that the CWT method does detect melting over an equivalent extent until several weeks later. This general tendency of the CWT to omit large scale early and late season melting events accounts for a greater estimated mean MI, 4 % larger than the FT3 method. This difference in MI is greatest for low elevation areas and generally decreases with higher elevations. This indicates that a majority of sporadic, large-scale, melting events occur for low elevation ice-shelf regions and that at higher elevations melting is rapid melt/refreeze cycles similar to the Dronning Maude Land.

From a comparison with AWS, we find that overall the FT3 has higher level of agreement with the temperature measurements with a 66 % total accuracy compared to the 54 % from the CWT method. This is true for all AWS, apart from the Pegasus South Station where the CWT has a 10 % greater accuracy than the FT3 method. The FT3 method has a better accuracy in general because of its ability to measure short duration melting events that are common for several stations (e.g. Limbert). For the Pegasus South AWS, it appears that the melting season occurs with a relatively low loss in

backscatter, it is therefore never consistently under the 3 dB threshold. This lowers the accuracy of the FT3 method, but does not affect the CWT approach. However many of these above-zero temperature events are not long-lasting in nature, and to evaluate the CWT method solely using accuracy assessments does not indicate the true utility of this approach: to create a record of sustained melting events.

Compared to M + 30 K, a PMW derived approach; both AMW melting records find a similar yearly MI, where the FT3 is within 11 % and the CWT within 9 % relative difference. These methods find a greater level of disagreement with a dynamic thresholding approach, MT09. The CWT methods find a greater overall agreement in temporal trend for both PMW methods, for the M + 30 K method $r = 0.943$ ($p < 0.001$) with CWT and $r = 0.922$ ($p = 0.001$) for the FT3 method. Spatially, we find that comparison is dominated by a mixed pixel effect, making it difficult to determine the difference between melt duration on a per-pixel basis. The FT3 method has a higher degree of spatial autocorrelation with PMW (M + 30 K) approaches than the CWT, with significant variability in AMW derived MD for similar PMW measurements. Since PMW pixels are ~ 10 times the scale of the spatially enhanced QuikSCAT product we attribute this variability to mixed pixel effects. Based on the strong correlation in yearly MI totals, the differences in spatial variability appear to be averaged out over the total area.

This method also has utility in the analysis of sustained melting events and large scale climate indicators such as the SAM. It is apparent that by looking at only sustained melting events, we are able to show linkages with SAM indices not detected using threshold based approaches. These findings agree with the notion of increased melting during positive SAM anomalies during overflow conditions.

Acknowledgements. The authors acknowledge the support of NSF grant ANT-1141993. The authors acknowledge David Long and the NASA Jet Propulsion Laboratory PO.DAAC for providing the enhanced resolution scatterometer products. The authors appreciate the support of the Automatic Weather Station Program and/or the data set, data display, information, etc. (Matthew Lazzara, NSF grants number ARC0713843, ANT0944018, and/or ANT1141908). This research was supported, in part, under National Science Foundation Grants CNS-0958379

Wavelet Snowmelt Algorithm over Antarctica

N. Steiner and
M. Tedesco

[Title Page](#)

[Abstract](#)

[Introduction](#)

[Conclusions](#)

[References](#)

[Tables](#)

[Figures](#)

◀

▶

◀

▶

[Back](#)

[Close](#)

[Full Screen / Esc](#)

[Printer-friendly Version](#)

[Interactive Discussion](#)



References

- Abdalati, W. and Steffen, K.: Greenland ice sheet melt extent: 1979–1999, *J. Geophys. Res.-Atmos.*, 106, 33983–33988, doi:10.1029/2001jd900181, 2001.
- Alexandrescu, M., Gibert, D., Hulot, G., Lemouel, J. L., and Saracco, G.: Detection of geomagnetic jerks using wavelet analysis, *J. Geophys. Res.-Solid Earth*, 100, 12557–12572, doi:10.1029/95JB00314, 1995.
- Ashcraft, I. S. and Long, D. G.: Comparison of methods for melt detection over Greenland using active and passive microwave measurements, *Int. J. Remote Sens.*, 27, 2469–2488, doi:10.1080/01431160500534465, 2006.
- Barrand, N. E., Vaughan, D. G., Steiner, N., Tedesco, M., Munneke, P. K., Van den Broeke, M. R., and Hosking, J. S.: Trends in Antarctic Peninsula surface melting conditions from observations and regional climate modeling, *J. Geophys. Res.: Earth Surf.*, 118, 1–16, doi:10.1029/2012JF002559, 2013.
- Bromwich, D. H. and Nicolas, J. P.: Sea-Level Rise Ice-sheet uncertainty, *Nat. Geosci.*, 3, 596–597, doi:10.1038/ngeo946, 2010.
- Chen, J. L., Wilson, C. R., and Tapley, B. D.: Interannual variability of Greenland ice losses from satellite gravimetry, *J. Geophys. Res.-Solid Earth*, 116, B07406, doi:10.1029/2010jb007789, 2011.
- Comiso, J.: *Polar Oceans from Space*, Springer, New York., 2010.
- Daubechies, I.: *Ten Lectures on Wavelets*, Society for Industrial and Applied Mathematics, Philadelphia, PA, 1992.
- Dowdeswell, J. A.: Atmospheric science – the Greenland Ice Sheet and global sea-level rise, *Science*, 311, 963–964, doi:10.1126/science.1124190, 2006.
- Early, D. S. and Long, D. G.: Image reconstruction and enhanced resolution imaging from irregular samples, *IEEE T. Geosci. Remote*, 39, 291–302, doi:10.1109/36.905237, 2001.
- Le Gonidec, Y. and Gibert, D.: The wavelet response as a multiscale characterization of scattering processes at granular interfaces, *Ultrasonics*, 44, 381–390, doi:10.1016/j.ultras.2006.05.212, 2006.

Wavelet Snowmelt Algorithm over Antarctica

N. Steiner and
M. Tedesco

[Title Page](#)

[Abstract](#) [Introduction](#)

[Conclusions](#) [References](#)

[Tables](#) [Figures](#)

[◀](#) [▶](#)

[◀](#) [▶](#)

[Back](#) [Close](#)

[Full Screen / Esc](#)

[Printer-friendly Version](#)

[Interactive Discussion](#)



- Le Gonidec, Y., Gibert, D., and Proust, J. N.: Multiscale analysis of waves reflected by complex interfaces: basic principles and experiments, *J. Geophys. Res.-Solid Earth*, 107, 2184, doi:10.1029/2001JB000558, 2002.
- Hansen, J., Ruedy, R., Sato, M., and Lo, K.: Global surface temperature change, *Rev. Geophys.*, 48, Rg4004, doi:10.1029/2010rg000345, 2010.
- Herrmann, F. J.: Singularity characterization by monoscale analysis: application to seismic imaging, *Appl. Comput. Harmonic Anal.*, 11, 64–88, doi:10.1006/acha.2000.0349, 2001.
- Holland, P. R., Corr, H. F. J., Pritchard, H. D., Vaughan, D. G., Arthern, R. J., Jenkins, A., and Tedesco, M.: The air content of Larsen Ice Shelf, *Geophys. Res. Lett.*, 38, L10503, doi:10.1029/2011GL047245, 2011.
- Holschneider, M.: Wavelets: an Analysis Tool, Clarendon Press, Oxford University Press, Oxford, New York, 1995.
- Hughes, T. J.: The weak underbelly of the West Antarctic ice-sheet, *J. Glaciol.*, 27, 518–525, 1981.
- Joshi, M., Merry, C. J., Jezeck, K. C., and Bolzan, J. F.: An edge detection technique to estimate melt duration, season and melt extent on the Greenland ice sheet using passive microwave data, *Geophys. Res. Lett.*, 28, 3497–3500, doi:10.1029/2000GL012503, 2001.
- Joughin, I. and Alley, R. B.: Stability of the West Antarctic ice sheet in a warming world, *Nat. Geosci.*, 4, 506–513, doi:10.1038/ngeo1194, 2011.
- Van Lipzig, N. P. M., Marshall, G. J., Orr, A., and King, J. C.: The relationship between the Southern Hemisphere annular mode and Antarctic Peninsula summer temperatures: analysis of a high-resolution model climatology, *J. Climate*, 21, 1649–1668, doi:10.1175/2007JCLI1695.1, 2008.
- Lemke, P., Ren, J., Alley, R. B., Allison, I., Carrasco, J., Flato, G., Fujii, Y., Kaser, G., Mote, P., Thomas, R. H., and Zhang, T.: Observations: Changes in Snow, Ice and Frozen Ground, in: Climate change 2007: the physical science basis; summary for policymakers, technical summary and frequently asked questions, Part of the Working Group I contribution to the Fourth Assessment Report of the Intergovernmental Panel on Climate Change, ISBN: 9291691216, 2007.
- Liu, H., Wang, L., and Jezeck, K. C.: Wavelet-transform based edge detection approach to derivation of snowmelt onset, end and duration from satellite passive microwave measurements, *Int. J. Remote Sens.*, 26, 4639–4660, 2005.

Wavelet Snowmelt Algorithm over Antarctica

N. Steiner and
M. Tedesco

[Title Page](#)

[Abstract](#)

[Introduction](#)

[Conclusions](#)

[References](#)

[Tables](#)

[Figures](#)

◀

▶

◀

▶

[Back](#)

[Close](#)

[Full Screen / Esc](#)

[Printer-friendly Version](#)

[Interactive Discussion](#)



Wavelet Snowmelt Algorithm over Antarctica

N. Steiner and
M. Tedesco

Title Page

Abstract

Introduction

Conclusions

References

Tables

Figures

| <

Bac

Close

Full Screen / Esc

Long, D. G. and Hicks, B. R.: Standard BYU QuikScat/SeaWinds land/ice image products. Brigham Young Univ., Provo, UT, QuikScat Image Product documentation, 2000.

MacAyeal, D. R., Scambos, T. A., Hulbe, C. L., and Fahnestock, M. A.: Catastrophic ice-shelf break-up by an ice-shelf-fragment-capsize mechanism, *J. Glaciol.*, 49, 22–36, doi:10.3189/172756503781830863, 2003.

Mallat, S. G.: A Wavelet Tour of Signal Processing, 2nd Ed., Academic Press, San Diego, 1999.

Mallat, S. G. and Hwang, W. L.: Singularity detection and processing with wavelets, *IEEE T. Inform. Theor.*, 38, 617–643, doi:10.1109/18.119727, 1992.

Mallat, S. G. and Zhong, S.: Characterization of signals from multiscale edges, *IEEE T. Pattern Anal. Machine Int.*, 14, 710–732, doi:10.1109/34.142909, 1992.

Marshall, G. J.: Trends in the southern annular mode from observations and reanalyses, *J. Climate*, 16, 4134–4143, doi:10.1175/1520-0442(2003)016<4134:TITSAM>2.0.CO;2, 2003.

Mote, T. L. and Anderson, M. R.: Variations in snowpack melt on the Greenland ice-sheet based on passive-microwave measurements, *J. Glaciol.*, 41, 51–60, 1995.

Mote, T. L., Anderson, M. R., Kuivinen, K. C., and Rowe, C. M.: Passive microwave-derived spatial and temporal variations of summer melt on the Greenland ice sheet, *Ann. Glaciol.*, 17, 233–238, 1993.

Nghiem, S. V., Steffen, K., Kwok, R., and Tsai, W. Y.: Detection of snowmelt regions on the Greenland ice sheet using diurnal backscatter change, *J. Glaciol.*, 47, 539–547, doi:10.3189/172756501781831738, 2001.

Nghiem, S. V., Steffen, K., Neumann, G., and Huff, R.: Snow accumulation and snowmelt monitoring in Greenland and Antarctica, in: *Dynamic Planet*, Springer Berlin Heidelberg, 31–38, 2007.

Ohmura, A.: Physical basis for the temperature-based melt-index method, *J. Appl. Meteorol.*, 40, 753–761, doi:10.1175/1520-0450(2001)040<0753:pbfttb>2.0.co;2, 2001.

Overpeck, J. T., Otto-Bliesner, B. L., Miller, G. H., Muhs, D. R., Alley, R. B., and Kiehl, J. T.: Paleoclimatic evidence for future ice-sheet instability and rapid sea-level rise, *Science*, 311, 1747–1750, doi:10.1126/science.1115159, 2006.

Rignot, E. and Thomas, R. H.: Mass balance of polar ice sheets, *Science*, 297, 1502–1506, 2002.

Rignot, E., Casassa, G., Gogineni, P., Krabill, W., Rivera, A., and Thomas, R.: Accelerated ice discharge from the Antarctic Peninsula following the collapse of Larsen B ice shelf, *Geophys. Res. Lett.*, 31, L18401, doi:10.1029/2004GL020697, 2004.

- Rignot, E., Velicogna, I., Van den Broeke, M. R., Monaghan, A., and Lenaerts, J.: Acceleration of the contribution of the Greenland and Antarctic ice sheets to sea level rise, *Geophys. Res. Lett.*, 38, L05503, doi:10.1029/2011gl046583, 2011.
- Rott, H., Müller, F., Nagler, T., and Floricioiu, D.: The imbalance of glaciers after disintegration of Larsen-B ice shelf, Antarctic Peninsula, *The Cryosphere*, 5, 125–134, doi:10.5194/tc-5-125-2011, 2011.
- Scambos, T. A., Bohlander, J. A., Shuman, C. A., and Skvarca, P.: Glacier acceleration and thinning after ice shelf collapse in the Larsen B embayment, Antarctica, *Geophys. Res. Lett.*, 31, L18402, doi:10.1029/2004gl020670, 2004.
- Scambos, T., Fricker, H. A., Liu, C. C., Bohlander, J., Fastook, J., Sargent, A., Massom, R., and Wu, A. M.: Ice shelf disintegration by plate bending and hydro-fracture: satellite observations and model results of the 2008 Wilkins ice shelf break-ups, *Earth Planet. Sc. Lett.*, 280, 51–60, doi:10.1016/j.epsl.2008.12.027, 2009.
- Shepherd, A., Ivins, E. R., Geruo, A., Barletta, V. R., Bentley, M. J., Bettadpur, S., Briggs, K. H., Bromwich, D. H., Forsberg, R., and Galin, N.: A reconciled estimate of ice-sheet mass balance, *Science*, 338, 1183–1189, 2012.
- Shepherd, A. and Wingham, D.: Recent sea-level contributions of the Antarctic and Greenland ice sheets, *Science*, 315, 1529–1532, doi:10.1126/science.1136776, 2007.
- Spencer, M. W., Wu, C. L., and Long, D. G.: Improved resolution backscatter measurements with the SeaWinds pencil-beam scatterometer, *IEEE T. Geosci. Remote*, 38, 89–104, doi:10.1109/36.823904, 2000.
- Steffen, K., Nghiem, S. V., Huff, R., and Neumann, G.: The melt anomaly of 2002 on the Greenland Ice Sheet from active and passive microwave satellite observations, *Geophys. Res. Lett.*, 31, L20402, doi:10.1029/2004GL020444, 2004.
- Stiles, W. H. and Ulaby, F. T.: The active and passive microwave response to snow parameters. 1. Wetness, *J. Geophys. Res.-Oceans Atmos.*, 85, 1037–1044, doi:10.1029/JC085iC02p01037, 1980.
- Tedesco, M.: Assessment and development of snowmelt retrieval algorithms over Antarctica from K-band spaceborne brightness temperature (1979–2008), *Remote Sens. Environ.*, 113, 979–997, doi:10.1016/j.rse.2009.01.009, 2009.
- Tedesco, M. and Monaghan, A. J.: An updated Antarctic melt record through 2009 and its linkages to high-latitude and tropical climate variability, *Geophys. Res. Lett.*, 36, L18502, doi:10.1029/2009GL039186, 2009.

Wavelet Snowmelt Algorithm over Antarctica

N. Steiner and
M. Tedesco

[Title Page](#)

[Abstract](#)

[Introduction](#)

[Conclusions](#)

[References](#)

[Tables](#)

[Figures](#)



[Back](#)

[Close](#)

[Full Screen / Esc](#)

[Printer-friendly Version](#)

[Interactive Discussion](#)



**Wavelet Snowmelt
Algorithm over
Antarctica**N. Steiner and
M. Tedesco

- Tedesco, M., Abdalati, W., and Zwally, H. J.: Persistent surface snowmelt over Antarctica (1987–2006) from 19.35 GHz brightness temperatures, *Geophys. Res. Lett.*, 34, L18504, doi:10.1029/2007gl031199, 2007.
- Thompson, D. W. J. and Wallace, J. M.: Annular modes in the extratropical circulation. Part I: Month-to-month variability, *J. Climate*, 13, 1000–1016, doi:10.1175/1520-0442(2000)013<1000:AMITEC>2.0.CO;2, 2000.
- Torinesi, O., Fily, M., and Genthon, C.: Variability and trends of the summer melt period of Antarctic ice margins since 1980 from microwave sensors, *J. Climate*, 16, 1047–1060, doi:10.1175/1520-0442(2003)016<1047:VATOTS>2.0.CO;2, 2003.
- Trusel, L. D., Frey, K. E., and Das, S. B.: Antarctic surface melting dynamics: enhanced perspectives from radar scatterometer data, *J. Geophys. Res.-Earth Surf.*, 117, doi:10.1029/2011JF002126, 2012.
- Ulaby, F. T., Moore, R. K., and Fung, A. K.: *Microwave Remote Sensing: Active and Passive Volume II: Radar Remote Sensing and Surface Scattering and Emission Theory*, Artech House, Ann Arbor, 1982.
- Ulaby, F. and Stiles, W. H.: The active and passive microwave response to snow parameters 2: water equivalent of dry snow, *J. Geophys. Res.-Oceans Atmos.*, 85, 1045–1049, doi:10.1029/JC085iC02p01045, 1980.
- Van den Broeke, M.: Strong surface melting preceded collapse of Antarctic Peninsula ice shelf, *Geophys. Res. Lett.*, 32, L12815, doi:10.1029/2005gl023247, 2005.
- Van den Broeke, M., Bus, C., Ettema, J., and Smeets, P.: Temperature thresholds for degree-day modelling of Greenland ice sheet melt rates, *Geophys. Res. Lett.*, 37, L18501, doi:10.1029/2010gl044123, 2010.
- Vaughan, D. G.: Recent trends in melting conditions on the Antarctic Peninsula and their implications for ice-sheet mass balance and sea level, *Arct. Antarct. Alp. Res.*, 38, 147–152, doi:10.1657/1523-0430(2006)038[0147:rtimco]2.0.co;2, 2006.
- Wang, L., Derksen, C., and Brown, R.: Detection of pan-Arctic terrestrial snowmelt from QuikSCAT, 2000–2005, *Remote Sens. Environ.*, 112, 3794–3805, doi:10.1016/j.rse.2008.05.017, 2008.
- Wang, L. and Yu, J.: Spatiotemporal segmentation of spaceborne passive microwave data for change detection, *IEEE Geosci. Remote.*, 8, 909–913, doi:10.1109/LGRS.2011.2140312, 2011.

Discussion Paper | Discussion Paper

[Title Page](#)[Abstract](#)[Introduction](#)[Conclusions](#)[References](#)[Tables](#)[Figures](#)[◀](#)[▶](#)[Back](#)[Close](#)[Full Screen / Esc](#)[Printer-friendly Version](#)[Interactive Discussion](#)

Weng, H. Y. and Lau, K. M.: Wavelets, period-doubling, and time-frequency localization with application to organization of convection over the Tropical Western Pacific, *J. Atmos. Sci.*, 51, 2523–2541, doi:10.1175/1520-0469(1994)051<2523:WPDATL>2.0.CO;2, 1994.

Zwally, H. J. and Fiegles, S.: Extent and duration of Antarctic surface melting, *J. Glaciol.*, 40, 463–476, 1994.

5

TCD

7, 2635–2678, 2013

Wavelet Snowmelt Algorithm over Antarctica

N. Steiner and
M. Tedesco

[Title Page](#)

[Abstract](#)

[Introduction](#)

[Conclusions](#)

[References](#)

[Tables](#)

[Figures](#)

◀

▶

[Back](#)

[Close](#)

[Full Screen / Esc](#)

[Printer-friendly Version](#)

[Interactive Discussion](#)



Wavelet Snowmelt Algorithm over Antarctica

N. Steiner and
M. Tedesco

Table 1. Stations used in the AWS evaluation. The agreement (true-positive), omission (false-positive), and commission (true-negative) relative differences from the comparison of melting estimated from AWS air temperatures and melt duration (MD) time-series estimated using the FT3 and CWT melt algorithms.

AWS station name	Accuracy		Omission Error				Commission Error	
	FT3	CWT	FT3	CWT	FT3	CWT	FT3	CWT
Butler Island	50 %	(92/184)	30 %	(55/184)	50 %	(92/184)	70 %	(129/184)
Fossil Bluff	75 %	(123/164)	66 %	(109/164)	25 %	(41/164)	34 %	(55/164)
Larsen Ice Shelf	87 %	(413/477)	77 %	(366/477)	13 %	(64/477)	23 %	(111/477)
Limbert	60 %	(21/35)	17 %	(6/35)	40 %	(14/35)	83 %	(29/35)
Pegasus South	38 %	(46/121)	48 %	(58/121)	62 %	(75/121)	52 %	(63/121)
Uranus Glacier	36 %	(57/160)	17 %	(27/160)	64 %	(103/160)	83 %	(133/160)
Total	66 %	(752/1141)	54 %	(621/1141)	34 %	(389/1141)	46 %	(520/1141)
							3 %	(467/13689)
							3 %	(401/13689)

- [Title Page](#)
- [Abstract](#) | [Introduction](#)
- [Conclusions](#) | [References](#)
- [Tables](#) | [Figures](#)
- [◀](#) | [▶](#)
- [◀](#) | [▶](#)
- [Back](#) | [Close](#)
- [Full Screen / Esc](#)
- [Printer-friendly Version](#)
- [Interactive Discussion](#)

Wavelet Snowmelt Algorithm over Antarctica

N. Steiner and
M. Tedesco

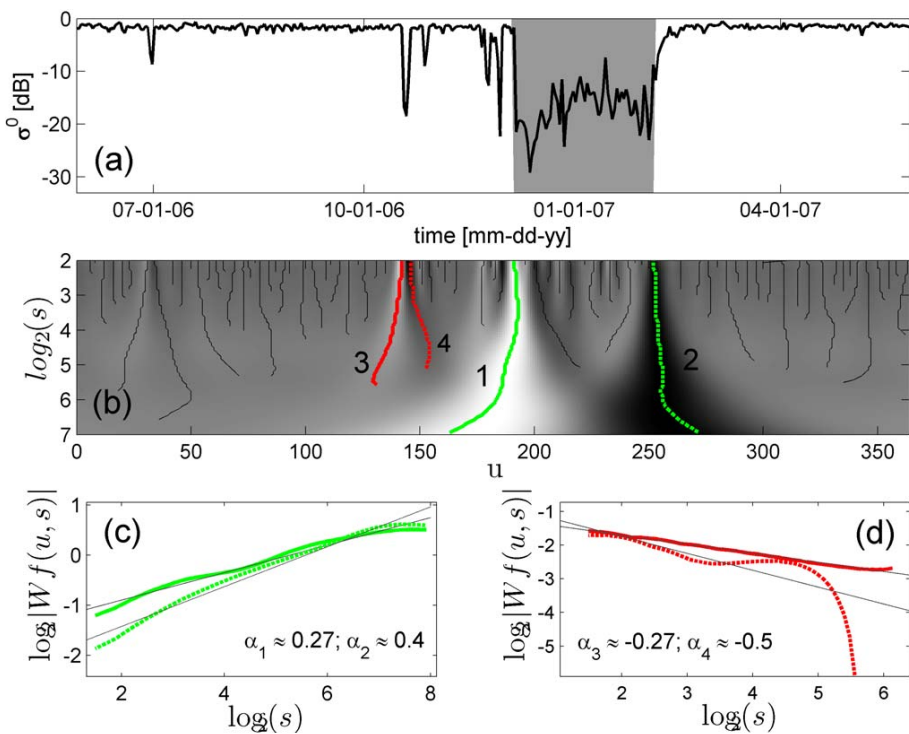


Fig. 1. (a) QuikSCAT σ^0 time-series with the melt duration (MD) estimated using the CWT method shaded in gray. (b) The CWT of the time series in (a) where dark gray to black colour values indicate positive $W\sigma^0$ and light-grey to white negative. WTMM1 are indicated as black, green or red lines associated with melt onset (MO, WTMM1) melt refreeze (MF, WTMM1 2) and sporadic, early season melt (WTMM1 3, WTMM1 4). (c) The $W\sigma^0$ along WTMM1 plotted over all scales, (s) and the associated α for the MO and MF events. (d) Same as (c) for an early season sporadic melting.

[Title Page](#)

[Abstract](#)

[Introduction](#)

[Conclusions](#)

[References](#)

[Tables](#)

[Figures](#)

◀

▶

[Back](#)

[Close](#)

[Full Screen / Esc](#)

[Printer-friendly Version](#)

[Interactive Discussion](#)

Wavelet Snowmelt Algorithm over Antarctica

N. Steiner and
M. Tedesco

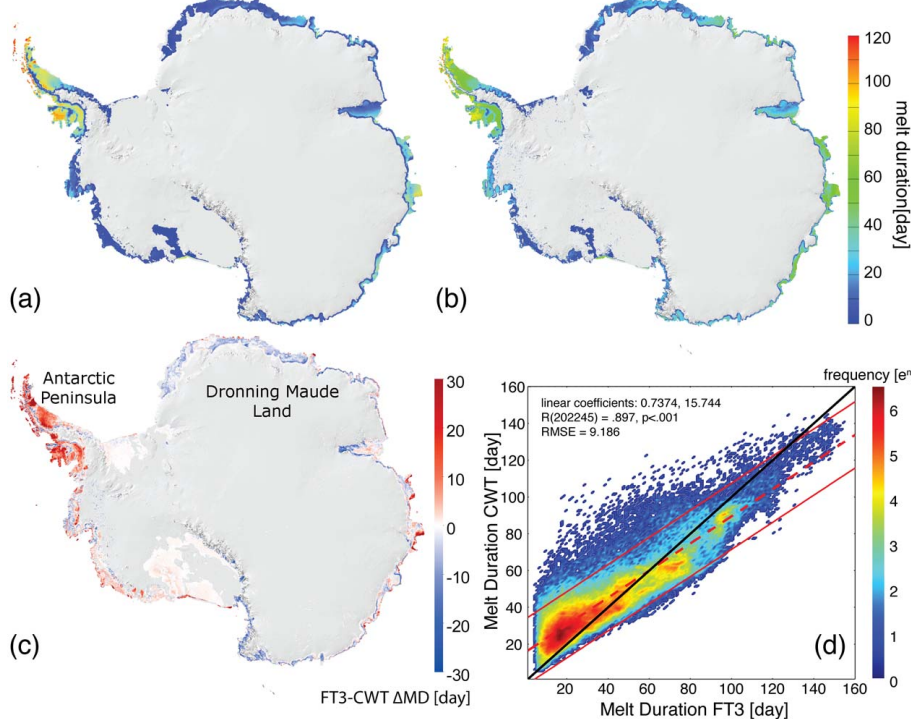


Fig. 2. (a) A map of mean (2000 through 2009) seasonal melt duration estimated from the Sea-Winds sensor on QuikScat, using a 3 dB below winter mean threshold (FT3) (b) and a continuous wavelet based method (CWT). (c) The difference between mean MD from both methods is indicated as Δ MD (FT3-CWT). The location of the Antarctic Peninsula (AP) and Dronning Maude Land (D) are labeled. (d) Autocorrelation analysis using a log transformed 2-axis histogram, where mean MD is compared for all areas where melt is detected by both methods.

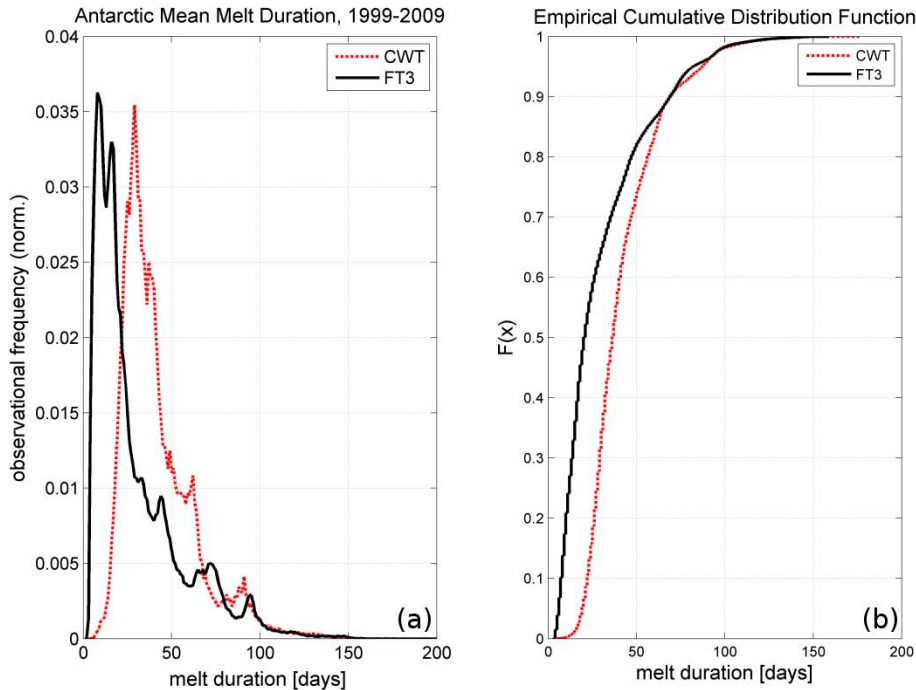
**Wavelet Snowmelt
Algorithm over
Antarctica**N. Steiner and
M. Tedesco

Fig. 3. (a) A histogram of all observed seasonal melt duration in days for the years 2000 through 2009 for the wavelet-based melt detection method (CWT) and a fixed threshold method (FT3). It is found that the observations for the CWT are shifted towards longer durations due to the exclusion of short duration melting events. (b) An empirical cumulative density function of observed melting duration.

Discussion Paper | Discussion Paper

[Title Page](#)[Abstract](#)[Introduction](#)[Conclusions](#)[References](#)[Tables](#)[Figures](#)[|◀](#)[▶|](#)[◀](#)[▶](#)[Back](#)[Close](#)[Full Screen / Esc](#)[Printer-friendly Version](#)[Interactive Discussion](#)

Wavelet Snowmelt Algorithm over Antarctica

N. Steiner and
M. Tedesco

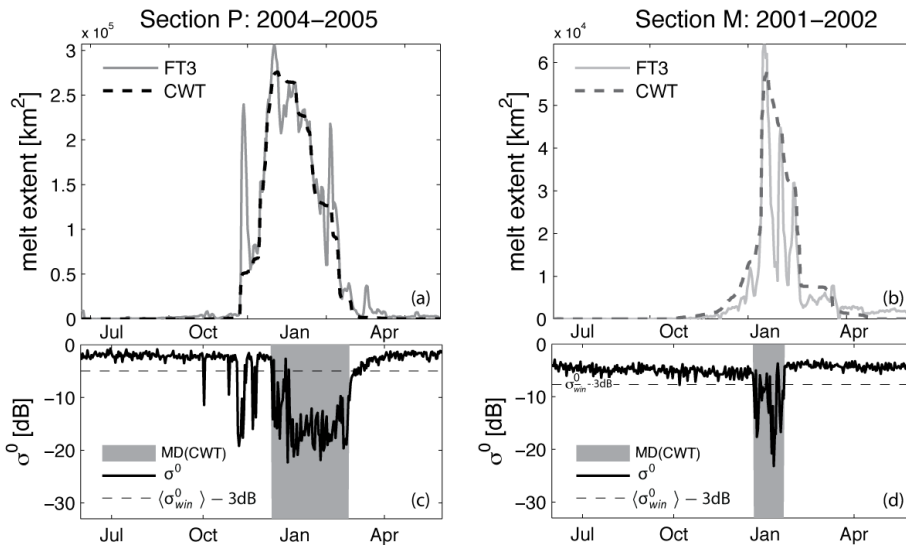


Fig. 4. (a) A time-series of total integrated melt extent for 2004–2005 estimated using the FT3 and CWT methods over the Antarctic Peninsula (Section P) and (b) during the 2001–2002 melting season for the Dronning Maude Land (Section M). Backscattering time-series are plotted for (c) a representative pixel location for the Antarctic Peninsula during the 2004–2005 austral summer and (d) Dronning Maude Land during the 2001–2002 austal summer to illustrate the results of melt classification by of CWT (shaded) and FT3 methods (threshold indicated).

[Title Page](#)

[Abstract](#)

[Introduction](#)

[Conclusions](#)

[References](#)

[Tables](#)

[Figures](#)

[◀](#)

[▶](#)

[Back](#)

[Close](#)

[Full Screen / Esc](#)

[Printer-friendly Version](#)

[Interactive Discussion](#)

Wavelet Snowmelt Algorithm over Antarctica

N. Steiner and
M. Tedesco

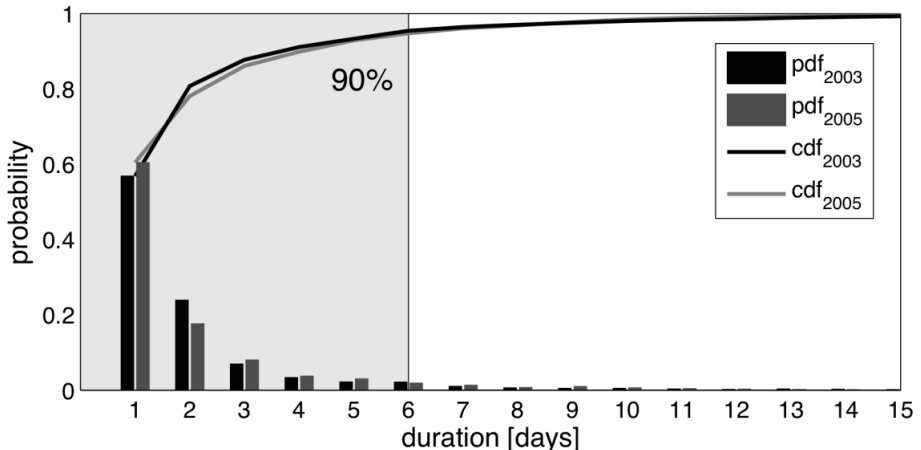


Fig. 5. The empirical probability density function (bar) and cumulative density function (line) of continuous melting periods per season observed over Antarctica (not the total per-pixel seasonal difference) for the 2003–2004 and 2005–2006 season that are found using a FT3 but rejected in by CWT.

Wavelet Snowmelt Algorithm over Antarctica

N. Steiner and
M. Tedesco

[Title Page](#)

[Abstract](#)

[Introduction](#)

[Conclusions](#)

[References](#)

[Tables](#)

[Figures](#)

[◀](#)

[▶](#)

[◀](#)

[▶](#)

[Back](#)

[Close](#)

[Full Screen / Esc](#)

[Printer-friendly Version](#)

[Interactive Discussion](#)

Wavelet Snowmelt Algorithm over Antarctica

N. Steiner and
M. Tedesco

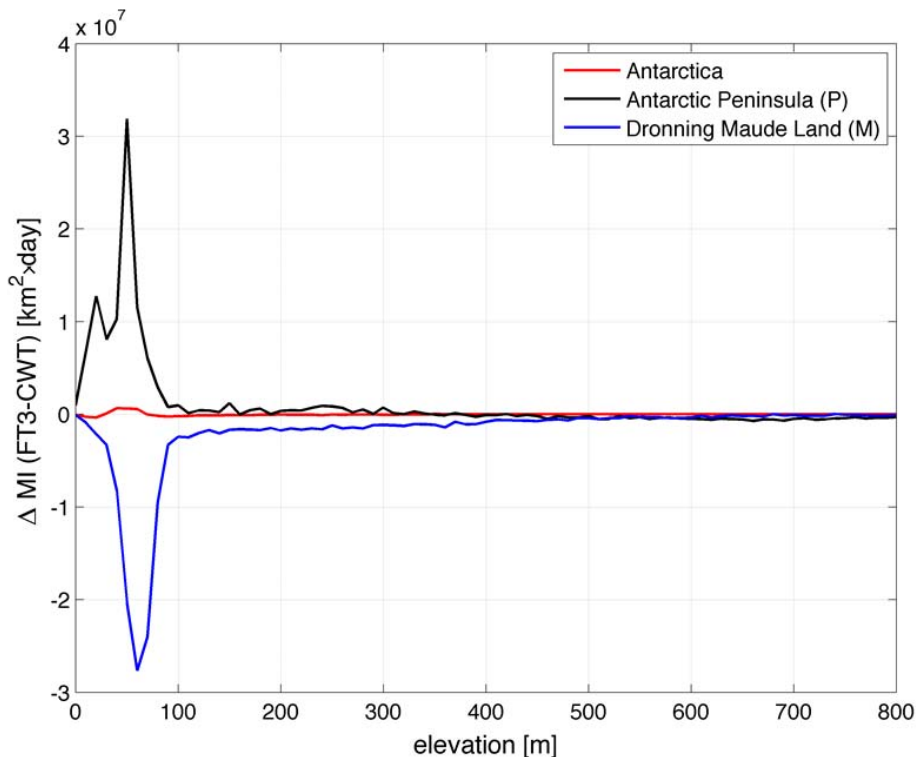


Fig. 6. An analysis of the difference in melting index ($\Delta MI = MI_{FT3} - MI_{CWT}$) estimates from the FT3 and CWT methods at a range of elevations for the entire Antarctic continent (red line) as well as the Antarctic Peninsula (black line) and Dronning Maude Land (blue line).

[Title Page](#)[Abstract](#)[Introduction](#)[Conclusions](#)[References](#)[Tables](#)[Figures](#)[◀](#)[▶](#)[◀](#)[▶](#)[Back](#)[Close](#)[Full Screen / Esc](#)[Printer-friendly Version](#)[Interactive Discussion](#)

Wavelet Snowmelt Algorithm over Antarctica

N. Steiner and
M. Tedesco

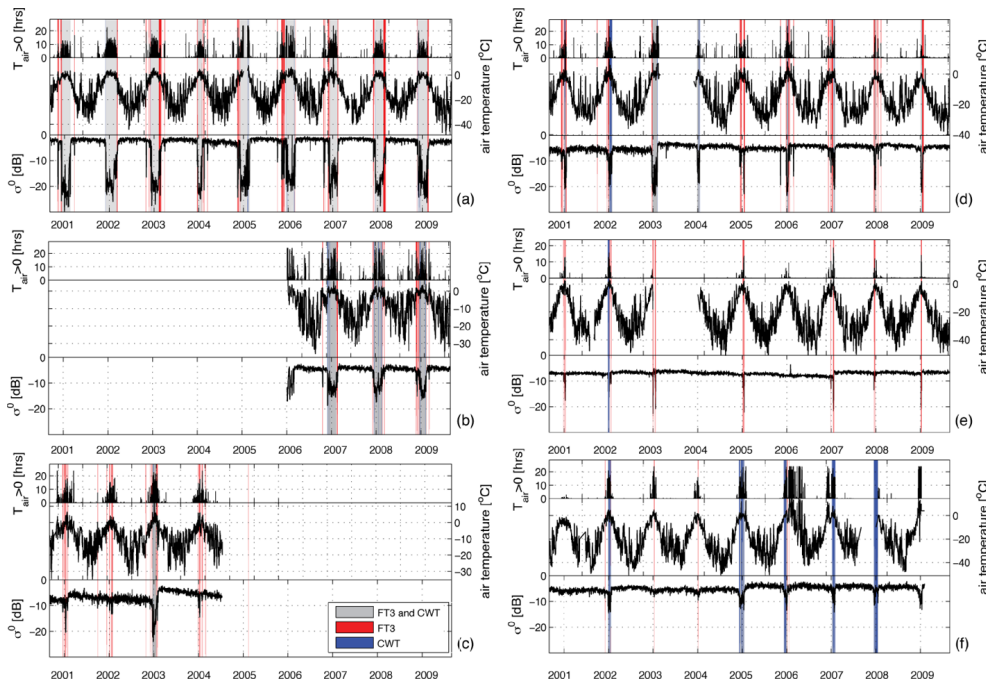


Fig. 7. AWS temperature records for the **(a)** Larsen Ice Shelf, **(b)** the Fossil Bluff, **(c)** the Uranus Glacier, **(d)** Butler Island, **(e)** Limbert and **(f)** Pegasus South for 2000 to 2009 plotted with the corresponding QuikSCAT backscattering values. Times where the FT3 or CWT approaches estimate melting are shaded red and blue respectively, while times where both methods agree are shaded grey.

[Title Page](#)

[Abstract](#)

[Introduction](#)

[Conclusions](#)

[References](#)

[Tables](#)

[Figures](#)



[Back](#)

[Close](#)

[Full Screen / Esc](#)

[Printer-friendly Version](#)

[Interactive Discussion](#)

Wavelet Snowmelt Algorithm over Antarctica

N. Steiner and
M. Tedesco

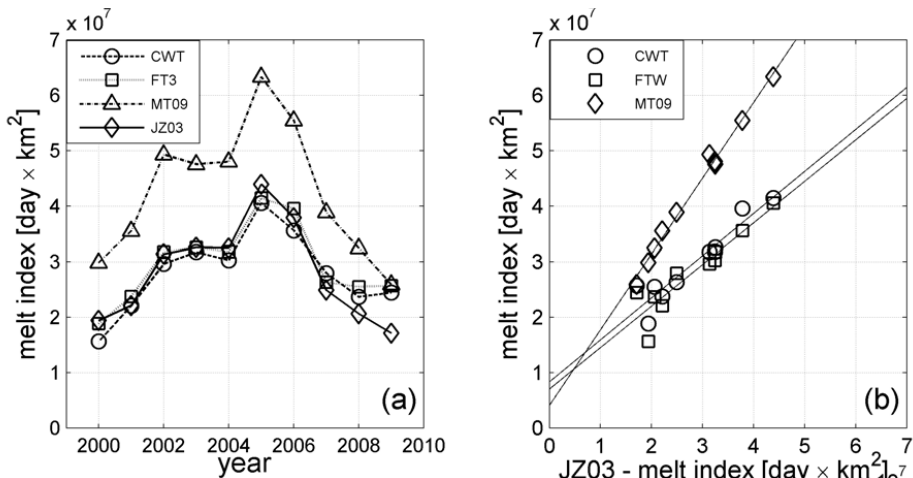


Fig. 8. (a) The time series of total melt index (MI), in $\text{day} \text{km}^{-2}$ for the Antarctic continent plotted for the years 1999 through 2009 derived from the FT3 and CWT methods on an enhanced resolution QuikSCAT active microwave dataset along with estimates from the MEMLS and M + 30 K methods and a SSM/I dataset. (b) The correlation between the FT3, QuikSCAT dataset MI estimates and the CWT, M + 30 K and MEMLS methods indicated using a linear regression.

[Title Page](#)

[Abstract](#)

[Introduction](#)

[Conclusions](#)

[References](#)

[Tables](#)

[Figures](#)

[◀](#)

[▶](#)

[Back](#)

[Close](#)

[Full Screen / Esc](#)

[Printer-friendly Version](#)

[Interactive Discussion](#)

Wavelet Snowmelt Algorithm over Antarctica

N. Steiner and
M. Tedesco

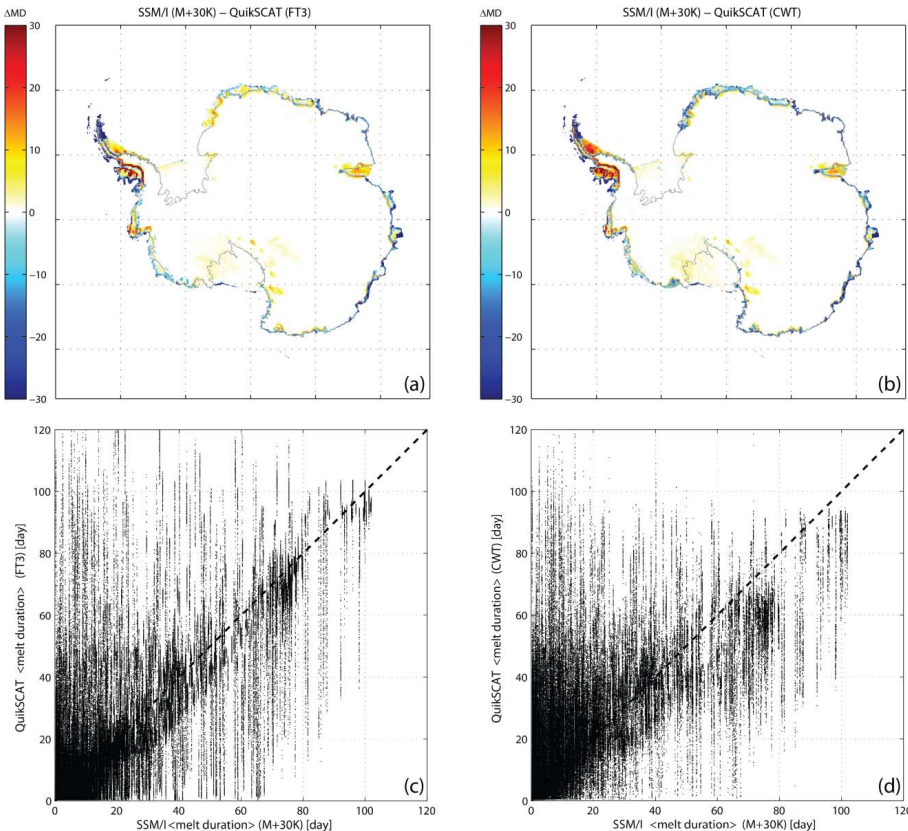


Fig. 9. The difference in average melt duration ($\Delta MD = MD_{SSM/I} - MD_{QuikSCAT}$), over the period of 1999–2009, between the up-sampled passive microwave SSM/I dataset, where melt is estimated using the M+K30 approach and the enhanced resolution QuikSCAT scatterometer dataset, where melt is estimated using the (a) FT3 and (b) CWT methods. Per-pixel scatterplots of average melt duration between SSM/I (M + 30 K) and the (c) FT3 and (d) CWT approaches.

[Title Page](#)

[Abstract](#)

[Introduction](#)

[Conclusions](#)

[References](#)

[Tables](#)

[Figures](#)

[◀](#)

[▶](#)

[◀](#)

[▶](#)

[Back](#)

[Close](#)

[Full Screen / Esc](#)

[Printer-friendly Version](#)

[Interactive Discussion](#)

Wavelet Snowmelt Algorithm over Antarctica

N. Steiner and
M. Tedesco

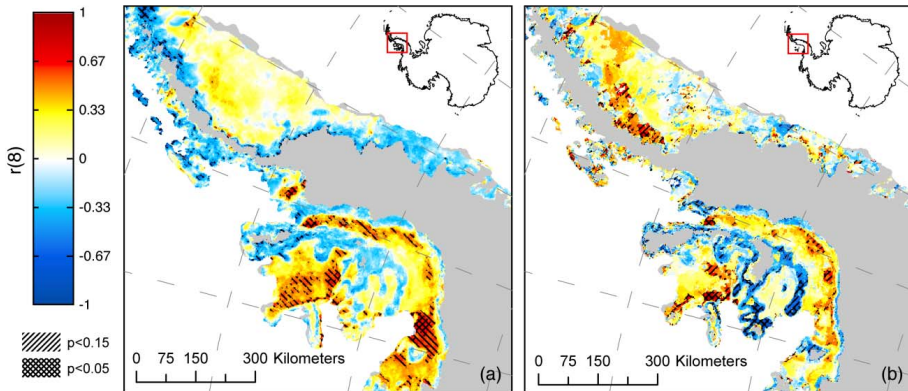


Fig. 10. Correlation, using the Pearson's coefficient, r , and the set of 9 melting years, between SAM (averaged for December, January, and February) and melt duration for the (a) FT3 method and (b) CWT. Areas with moderate or strong correlations are indicated with single hash ($p < 0.15$) and double hash marks ($p < 0.05$) respectively.

[Title Page](#)

[Abstract](#)

[Introduction](#)

[Conclusions](#)

[References](#)

[Tables](#)

[Figures](#)

◀

▶

◀

▶

[Back](#)

[Close](#)

[Full Screen / Esc](#)

[Printer-friendly Version](#)

[Interactive Discussion](#)